Journal of Alloys and Compounds 507 (2010) 29–32

Contents lists available at ScienceDirect

Journal of Alloys and Compounds

journal homepage: www.elsevier.com/locate/jallcom

Effect of Ba doping on magnetic and dielectric properties of nanocrystalline $BiFeO_3$ at room temperature

Chou Yang[a], Ji-Sen Jiang[a,*], Fang-Zhen Qian[a], Dong-Mei Jiang[a], Chun-Mei Wang[a], Wei-Guo Zhang[b]

[a] Department of Physics, Center of Functional Nanomaterials and Devices, East China Normal University, Shanghai 200241, People's Republic of China
[b] State Key Laboratory of Estuarine and Coastal Research, East China Normal University, Shanghai 200062, People's Republic of China

ARTICLE INFO

Article history:
Received 21 April 2010
Accepted 27 July 2010
Available online 5 August 2010

Keywords:
$BiFeO_3$
Nanocrystalline
Ba doping
Magnetic properties
Dielectric properties

ABSTRACT

Ba doped $BiFeO_3$ nanocrystallines were prepared by a sol–gel method. The crystal structure and morphology of the prepared samples were characterized using X-ray diffraction analysis and transmission electron microscope, respectively. The results showed that the lattice structure of the nanocrystallines transformed from rhombohedral to tetragonal with Ba substitution increased and the average grain size of the prepared samples lay in the range of 20–70 nm. Dielectric properties and magnetic properties of the nanocrystallines were studied. Dielectric properties were measured up to high frequency ~100 MHz. We found that suitable amount of Ba dopant was helpful to improve the dielectric properties of BFO and the nanocrystalline with 20% Ba doping on Bi sites had the best dielectric properties among the Ba doped nanocrystallines. Magnetic properties of the nanocrystallines were greatly improved due to the presence of oxygen deficiency and significant opening in the room-temperature M–H loop was observed with Ba substitution. All the nanocrystallines presented the high ratio of M_r/M from 0.462 to 0.594 and large coercivity from 3.92 to 5.16 kOe.

1. Introduction

Multiferroic materials, which simultaneously exhibit electric and magnetic ordering in same phase, have attracted a surge of interests due to their potential applications for the future technology in information storage [1], sensors [2,3], and for exploring physical phenomena in the coupling mechanism between electronic and magnetic order parameters [4]. However, most of the magnetic ferroelectrics usually have low magnetic transition temperature, which constricts the possibilities for their application. From this point of view, $BiFeO_3$ (BFO) with a distorted perovskite (ABO_3) structure becomes the most extensively studied multiferroic material because of its ferroelectric transition temperature ($T_c \sim 1100$ K) and antiferromagnetic Néel temperature ($T_N \sim 640$ K) well above the room-temperature (RT) [5]. The major problem is that the magnetic ordering of BFO has a spatially modulated spin structure [6], which does not allow net magnetization and inhibits the observation of the linear magnetoelectric effect [7]. Several groups have reported that the multiferroic properties of BFO with various ions substituted at A or/and B site can be improved [8–11]. And a common way to significantly increase the magnetization of the BFO is to substitute metal ions at A site of BFO with rare earth ions with large magnetic moment [9,10]. Recently, divalent cation (Ca, Sr, Pb, and Ba) substituted BFO ceramics prepared by solid-state reaction has been reported to exhibit enhanced magnetization [12,13]. Interestingly, the magnetic moment with divalent alkaline-earth metal substitution is comparable to that with the rare earth substituted BFO. Meanwhile, many researchers have reported that small particles enhanced magnetization of BFO and attributed it to the surface-induced magnetization [14,15] and ferromagnetism caused by apparent oxygen deficiency [16,17]. Moreover, with the miniaturization of electronic devices, it is both scientifically interesting and technologically challenging to synthesize and characterize an ultrafine, preferably nanosized BFO powders. So we expect to achieve larger magnetization through combining the cation effect of substituting ions and finite size effect of nanocrystalline. In this work, we utilized an ethylene glycol based sol–gel method to prepare $Bi_{1-x}Ba_xFeO_3$ ($x = 0.05$–0.30) nanocrystallines, and made a systematic study on the effect of Ba on the structure, dielectric and magnetic properties of BFO nanocrystalline at RT.

2. Experimental

The nanocrystallines of $Bi_{1-x}Ba_xFeO_3$ ($BBFO_x$) with $x = 0.05$, 0.10, 0.15, 0.20, 0.25, 0.30 respectively were synthesized by a sol–gel method. The starting materials were $Bi(NO_3)_3{\cdot}5H_2O$, $Fe(NO_3)_3{\cdot}9H_2O$, and $Ba(NO_3)_2$, which were of analytical grade and used without further purification. $Bi(NO_3)_3{\cdot}5H_2O$, $Fe(NO_3)_3{\cdot}9H_2O$, and $Ba(NO_3)_2$ were dissolved in ethylene glycol in proper stoichiometric proportions. The details of the preparation processing before annealing were given elsewhere [15]. The preheated powders annealed at 650 °C for 30 min. The crystal structure

* Corresponding author. Tel.: +86 21 54342940; fax: +86 21 54342940.
E-mail address: jsjiang@phy.ecnu.edu.cn (J.-S. Jiang).

0925-8388/$ – see front matter © 2010 Elsevier B.V. All rights reserved.
doi:10.1016/j.jallcom.2010.07.193

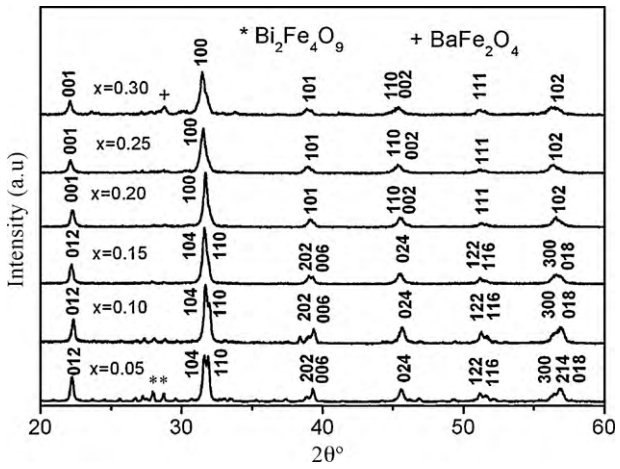

Fig. 1. Room temperature XRD patterns of $BBFO_x$ (x = 0.05, 0.10, 0.15, 0.20, 0.25, 0.30 respectively) samples.

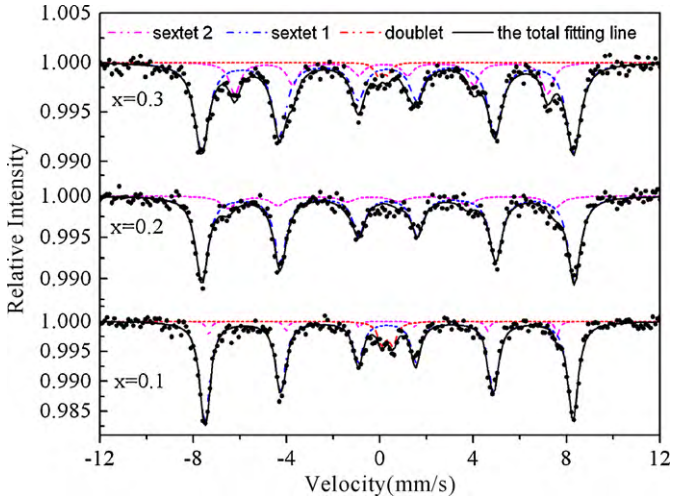

Fig. 3. RT Mössbauer spectra of the samples of $BBFO_x$ nanocrystallines.

Table 1
The unit cell parameters of $BBFO_x$.

Sample	d (size nm)	a (Å)	c (Å)	c/a	Crystalline structure
X = 0.05	63	5.64387	13.69272	2.4261	Rhombohedral
X = 0.10	47	5.63859	13.70418	2.4304	Rhombohedral
X = 0.15	41	5.64283	13.73763	2.4345	Rhombohedral
X = 0.20	28	2.81597	3.98477	1.4151	Tetragonal
X = 0.25	22	2.8288	3.99492	1.4122	Tetragonal
X = 0.30	20	2.82694	3.99074	1.4117	Tetragonal

and microstructural properties of $BBFO_x$ nanocrystallines were characterized at RT using X-ray diffraction (XRD) (D8 Advanced, Bruker, Karlsruhe, Germany) and transmission electron microscope (TEM) (JEOL, JEM 2100, Japan). The Mössbauer spectra were measured using a 12.5 mCi ^{57}Co (Pd) source, in a constant acceleration mode, and the spectra were calibrated by a 25 μm α-Fe foil at RT. The Mössbauer parameters were fitted by a standard least-squares fitting program. The dielectric properties of the samples were measured in the frequency range 20–100 MHz using a *LCR* HiTester (model HIOKI 3535, Japan). The magnetization hysteresis (M–H) loop was evaluated using a magnetic measurements variable field translation balance (MMVFTB) (model E, Peterson Instrument, Germany).

3. Results and discussions

Fig. 1 shows the XRD patterns of $BBFO_x$ (x = 0.05, 0.10, 0.15, 0.20, 0.25 and 0.30, respectively) at RT. The lattice parameters, the average grain sizes and crystalline structure associated with nanocrystalline $BBFO_x$ are summarized in Table 1. From the XRD analysis, a majority phase is $BBFO_x$ in the prepared samples. A small amount of $Bi_2Fe_4O_9$ exists along with the desired compound for x = 0.05, and this secondary phase vanishes for $x \geq 0.15$. In addition, an impurity phase ($BaFe_2O_4$) can be observed for x = 0.30. It is obvious that Ba substitution for Bi in BFO has affected the structure of the nanocrystalline from rhombohedral (x = 0.05, 0.10, 0.15) to tetragonal (x = 0.20, 0.25, 0.30). The tetragonal distortion (c/a) is decreased when Ba content increases from 0.2 to 0.3 in $BBFO_x$. The average grain sizes of the nanocrystallines were calculated from XRD peak broadening using the Debye–Schërrer equation. The grain size gradually decreases with increasing concentration of Ba. The trend was further supported by TEM characterization. Fig. 2 shows the TEM photographs of the samples for x = 0.05, 0.20, and 0.30, respectively.

The RT Mössbauer spectra of the nanocrystallines are shown in Fig. 3. The spectra are fitted to be two sextets and one doublet according to least-squares fitting program. The doublet of the sample for x = 0.10 suggests the existence of a paramagnetic impurity $Bi_2Fe_4O_9$ [18], and the doublet of the sample for x = 0.30 may be caused by the superparamagnetic effect of the ultrafine nanoparticles of the impurity $BaFe_2O_4$ [19]. The two sextets correspond to the Fe^{3+} ions of BFO in two different crystallographic environments [20]. According to Khomchenko et al. reports [12,13], when divalent cation replaces Bi^{3+}, charge balance in the compound is possible either by transforming a fraction of Fe^{3+} into Fe^{4+} or by creation of oxygen vacancy in the system. In the magnetically ordered phase, the valence of Fe should be mainly distinguished by the isomer shift (0.6–1.7 mm s^{-1} for Fe^{2+}, 0.05–0.5 mm s^{-1} for Fe^{3+} and −0.15–0.05 mm s^{-1} for Fe^{4+} (relative to the α-Fe standard)) [21]. The observed isomer shift values from RT Mössbauer date (0.34 and 0.22 for x = 0.10, 0.35 and 0.08 for x = 0.20, 0.32 and 0.31 for x = 0.30) clearly show the presence of Fe^{3+} state only. No signal of Fe^{4+} is detected in all the samples. Furthermore, according to Hodges' report [22], the isomer shift values of the spectra show that there exists non-octahedral coordination of Fe^{3+} in the $BBFO_x$. This indicates that charge balance in the compound is by creation of oxygen vacancy in the system. As for the values of quadrupole

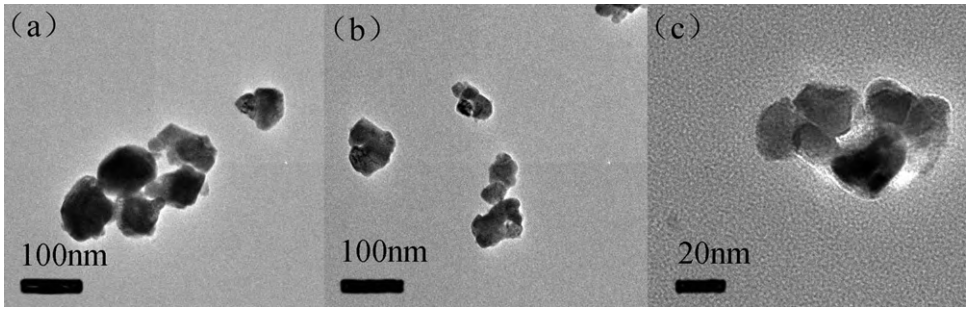

Fig. 2. TEM photographs of the samples of $BBFO_x$ nanoparticles: (a) x = 0.05, (b) x = 0.20 and (c) x = 0.30.

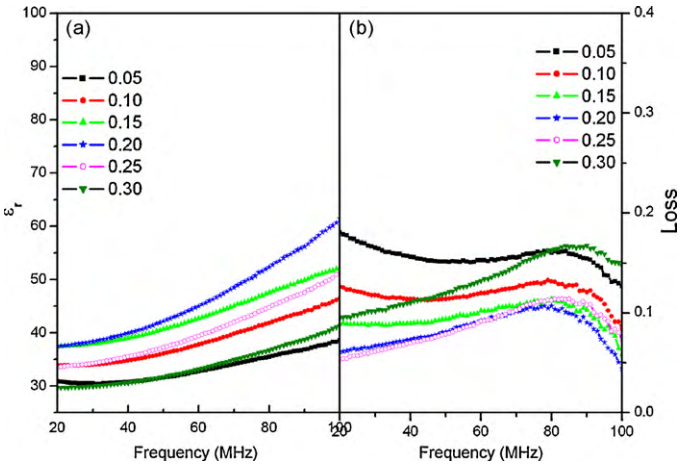

Fig. 4. Frequency dependence of (a) the dielectric constant and (b) loss for $BBFO_x$ nanocrystalline at RT.

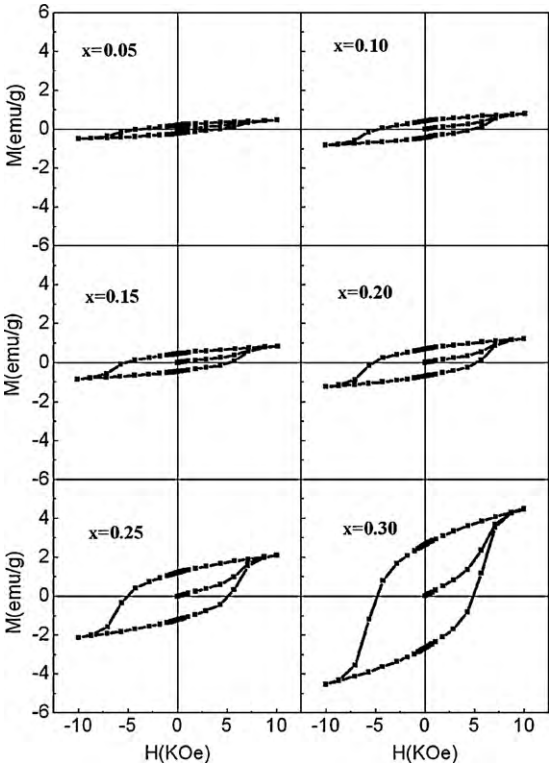

Fig. 5. *M–H* hysteresis loops of $BBFO_x$ nanocrystalline at RT.

splitting (Q.S.), there are some changes with increasing Ba content. When x was increased from 0.10 to 0.20, the value of Q.S. of sextet 1 changed from −0.08 to 0.01 mm/s and that of sextet 2 changed from 0.16 to −0.8 mm/s. These obvious changes in Q.S. suggest that there is a change in the crystallographic environments of Fe^{3+} ions in BFO while x was increased from 0.10 to 0.20. This corresponds to the lattice structure change from the rhombohedral structure to the tetragonal structure, as seen in XRD. But, there are only a few changes in Q.S. values (ΔQ.S = 0.01 mm/s) between two samples $x = 0.20$ and $x = 0.30$. This phenomenon confirms that the lattice structure of the sample for $x = 0.30$ is the same as that of the sample for $x = 0.20$. The tiny difference in the values of Q.S. corresponds to their different lattice parameters. In brief, the addition of Ba caused the change in the lattice structure and lattice parameters of BFO. These results are in agreement with those of XRD.

Fig. 4 shows the variation of relative dielectric constant and loss of the samples as a function of frequency (f). It can be observed from Fig. 4(a) that the dielectric constants of these samples increase with increasing frequency. The dispersions of dielectric constant of the samples are attributed to resonance effect, which may arise from the matching between the frequency of the mobility of charge carrier and that of the applied electric field [23]. Fig. 4(b) shows that the dielectric loss of the samples increases basically with the frequency increasing and then there appear to be a obvious resonance peak at about 80–90 MHz. It indicates that the position of resonance peaks can be controlled by the composition of the samples. Meanwhile, the dispersions of both the dielectric constant and dielectric loss of these samples with Ba content increasing can be divided into two trends. The dispersions of the samples for $x = 0.05$, 0.10, 0.15 are bracketed together, while those of the other three samples can be bracketed another. For dielectric constants, the samples with high Ba content ($x = 0.05, 0.10, 0.15$) show stronger dispersion than those of the samples with low Ba content. For dielectric loss, the samples with high Ba content increase with increasing frequency firstly and then decrease with increasing frequency, which is different from the samples with low Ba content. The difference may be caused by the change in crystalline structure. As seen from XRD, there existed a transition from the rhombohedral to tetragonal at $x = 0.20$. So we can draw a conclusion that the dispersion of the dielectric constant and loss of the samples have some connection with the change in crystalline structure.

Fig. 4 also shows that both the dielectric constant and dielectric loss of the samples regularly change with increasing Ba content. For low Ba content ($x = 0.05$, 0.10, 0.15), the dielectric constant of the samples increases and the dielectric loss of the samples decreases with increasing Ba content. This behavior can be qualitatively explained by interfacial polarization [24]. The space charges tend to accumulate around the interfaces between the face of the samples and the electrode under an applied electric field and form an interfacial layer with a high relative dielectric constant and a low dielectric loss, resulting in an increase in the relative dielectric constant and a decrease in the dielectric loss of the C/BFO/C capacitance. The space charges polarization increases with increasing oxygen vacancies, which increase with Ba content increasing. For high Ba content ($x = 0.20, 0.25, 0.30$), dielectric constant of samples decreases with Ba content increasing (Fig. 4(a)). This is similar to that of Fe-doped $BaTiO_3$ nanoparticles reported by Kundu et al. [25]. The dielectric constant with a tetragonal structure decreases with decreasing the c/a ratio, which decreases with increasing Ba content from the XRD analysis. It is evident from Fig. 4(b) that dielectric loss increases with Ba content increasing from 0.2 to 0.3 approximately. This can be attributed to the presence of impurities ($BaFe_2O_4$) and excess oxygen vacancy originated from Ba substitution in BFO. As discussed above, Ba dopant is helpful to improve the dielectric properties of BFO for low Ba content ($x = 0.05, 0.10, 0.15$), but the dielectric properties of BFO are suppressed with Ba content further increasing from $x = 0.20$ to 0.30. As a result, the dielectric properties of $BBFO_x$ for $x = 0.2$ is better than others.

Fig. 5 shows the *M–H* hysteresis loops of $BBFO_x$ nanocrystalline at RT. It is obvious that nonzero remnant magnetization (M_r) and coercive field (H_c) are observed for all samples. The magnetization curves were not saturated with the field up to 10 kOe. Magnetic parameters associated with nanocrystalline $BBFO_x$ were summarized in Table 2. It is observed that the H_c of the samples increases with increasing Ba content firstly and then decreases with increasing Ba content, which is may be caused by the change in crystalline structure. The H_c of $BBFO_x$ nanocrystalline were higher than that of the ceramic samples of $BBFO_x$ reported in Refs. [26,27] at the same doping concentration. Such high coercivity may be caused by the magnetic anisotropy. Compared to some doped BFO nanopar-

Table 2
Derived room-temperature magnetic parameters.

Sample	Size (nm)	M at 10 kOe (emu/g)	H_c (kOe)	M_r (emu/g)	M_r/M
$X = 0.05$	63	0.466	3.92	0.215	0.462
$X = 0.10$	47	0.807	4.92	0.432	0.535
$X = 0.15$	41	0.834	5.01	0.447	0.536
$X = 0.20$	28	1.242	5.16	0.699	0.563
$X = 0.25$	22	2.118	5.09	1.210	0.571
$X = 0.30$	20	4.512	4.77	2.681	0.594

ticles [28,29], $BBFO_x$ exhibits larger magnetization at 10 kOe, M_r and M_r/M at room temperature. The M_r and M_r/M increase with reduction in particle size. Due to the presence of Fe^{3+} state only from the RT Mössbauer spectra of the samples, the main reason for the increase in the magnetization cannot be attributed to valence fluctuation of Fe ions in BFO, but apparent oxygen deficiency. The origin of spontaneous magnetization can be explained in the following way. Firstly, the divalent Ba substitution in Bi site requires charge compensation, which is achieved by oxygen deficiency [30]. The oxygen deficiency increases with Ba content increasing. Secondly, BFO with the rhombohedral distorted perovskite structure allows a weak ferromagnetic ordering due to canting of the spins, with Ba doping the structure of $BBFO_x$ changes from rhombohedral to tetragonal and the bond angle of Fe–O–Fe may be changed, resulting in the magnetization of $BBFO_x$. As discussed above, Ba dopant in BFO greatly improve the magnetic properties of $BBFO_x$ and magnetic properties can be tuned by controlling Ba content.

4. Conclusions

In conclusion, $BBFO_x$ ($x = 0.05$, 0.10, 0.15, 0.20, 0.25 and 0.30, respectively) nanocrystallines have successfully been prepared by an ethylene glycol based sol–gel method. The average grain sizes of the samples for $x = 0.05$, 0.10, 0.15, 0.20, 0.25 and 0.30 were 63 nm, 47 nm, 41 nm, 28 nm, 22 nm and 20 nm, respectively. It was found that the lattice structure transformed from rhombohedral to tetragonal with Ba substitution increasing. The dispersion of the dielectric constant and loss of samples have some connection with the change in crystalline structure. With the transformation of crystal structure, the dispersion of the dielectric constant and loss of samples were changed. The dielectric constants of $BBFO_x$ increased and the dielectric loss decreased when Ba content increased from $x = 0.05$ to $x = 0.15$. When Ba content further increased, the change tendency of the dielectric properties of $BBFO_x$ with Ba content was opposite to that of the samples with low Ba content. Among these samples, $BBFO_x$ for $x = 0.2$ showed the largest dielectric constants and the lowest dielectric loss. The Ba doping in the antiferromagnetic BFO greatly improved the magnetic properties of $BBFO_x$. Significant opening in the room-temperature (RT) M–H loop was observed in the samples with Ba substitution. The enhancement of magnetization could not be attributed to the presence of Fe^{2+} but oxygen deficiency. Both the remnant magnetization (M_r) and magnetization (M at 10 kOe) increased with increasing Ba content. All the samples presented the high ratios of M_r/M and large coercivities. Especially for the sample of $x = 0.30$, it was of $M_r = 2.68$ emu/g and $M_r/M = 0.594$ at 10 kOe. This suggests that the $BBFO_x$ nanocrystalline is promising for applications in data-storage media.

Acknowledgments

This work was supported by Shanghai Nanotechnology Promotion Center (Grant No. 0852 nm03200), Ph.D. Program Scholarship Fund of ECNU 2009 (52YB2010), and Equipment Sharing Platform of ECNU.

References

[1] J. Hemberger, P. Lunkenheimer, R. Fichtl, H.A. Nidda, V. Tsurkan, A. Loidl, Nature (London) 434 (2005) 364–367.
[2] N.A. Hill, J. Phys. Chem. B 104 (2000) 6694–6709.
[3] W. Eerenstein, N.D. Mathur, J.F. Scott, Nature 442 (2006) 759–765.
[4] J.H. Xu, H. Ke, D.C. Jia, W. Wang, Y. Zhou, J. Alloys Compd. 472 (2009) 473–477.
[5] W. Prellier, M.P. Singh, P. Murugavel, J. Phys.: Condens. Matter 17 (2005) R803–R832.
[6] I. Sosnowska, T. Peterlin-Neumaier, E. Steichele, J. Phys. C 15 (1982) 4835–4846.
[7] Yu.F. Popov, A.K. Zvezdin, G.P. Vorob'ev, A.M. Kadomtseva, V.A. Murashev, D.N. Rakov, JETP Lett. 57 (1993) 69.
[8] F.Z. Qian, J.S. Jiang, S.Z. Guo, D.M. Jiang, W.G. Zhang, J. Appl. Phys. 106 (2009) 084312.
[9] V.R. Palkar, D.C. Kunkaliya, S.K. Malik, S. Bhattacharya, Phys. Rev. B 69 (2004) 212102.
[10] G.L. Yuan, S.W. Or, J. Appl. Phys. 100 (2006) 024109.
[11] Q. Xu, H. Zai, D. Wu, T. Qiu, M.X. Xu, Appl. Phys. Lett. 95 (2009) 112510.
[12] V.A. Khomchenko, D.A. Kiselev, J.M. Vieira, Li Jian, A.L. Kholkin, A.M.L. Lopes, Y.G. Pogorelov, J.P. Araujo, M. Maglione, J. Appl. Phys. 103 (2008) 024105.
[13] V.A. Khomchenko, D.A. Kiselev, J.M. Vieira, A.L. Kholkin, Y.G. Pogorelov, M.A. Sa, Appl. Phys. Lett. 90 (2007) 242901.
[14] G.C. Papaefthymiou, A.J. Viescas, A.R. Moodenbaugh, S.S. Wong, Nano Lett 7 (2007) 766–772.
[15] F.Z. Qian, J.S. Jiang, D.M. Jiang, W.G. Zhang, J.H. Liu, J. Phys. D: Appl. Phys. 43 (2010) 025403.
[16] R. Mazumder, P. Sujatha Devi, D. Bhattacharya, P. Choudhury, A. Sen, M. Raja, Appl. Phys. Lett. 91 (2007) 062510.
[17] S. Shetty, V.R. Palkar, R. Pinto, Pramana J. Phys. 58 (2002) 1027–1030.
[18] Z.W. Yu, H.Y. Miao, G.Q. Tan, Chin. J. Inorg. Chem. 24 (2008) 483–486.
[19] U. Topal, J. Magn. Magn. Mater. 320 (2008) 331–335.
[20] V.A. Khomchenko, D.A. Kiselev, J.M. Vieira, R.M. Rubinger, N.A. Sobolev, M. Kopcewicz, V.V. Shvartsman, P. Borisov, W. Kleemann, A.L. Kholkin, J. Phys.: Condens. Matter 20 (2008) 155207–155212.
[21] J.P. Hodges, S. Short, J.D. Jorgensen, X. Xiong, B. Dabrovski, S.M. Mini, C.W. Kimball, J. Solid State Chem. 151 (2000) 190–209.
[22] N.N. Greenwood, T.C. Gibb, Mössbauer Spectroscopy, Chapman and Hall, London, 1971.
[23] K.C. Verma, R.K. Kotnala, N.S. Negi, Appl. Phys. Lett. 92 (2008) 152902.
[24] X.Y. Zhang, Q. Song, F. Xu, C.K. Ong, Appl. Phys. Lett. 94 (2009) 022907.
[25] T.K. Kundu, A. Jana, P. Barik, Bull. Mater. Sci. 31 (2008) 501–505.
[26] V.A. Khomchenko, D.A. Kiselev, E.K. Selezneva, J.M. Vieira, A.M.L. Lopes, Y.G. Pogorelov, J.P. Araujo, A.L. Kholkin, Mater. Lett. 62 (2008) 1927–1929.
[27] V.B. Naik, R. Mahendiran, Solid State Commun. 149 (2009) 754–758.
[28] R.K. Mishra, D.K. Pradhan, R.N.P. Choudhary, A. Banerjee, J. Magn. Magn. Mater. 320 (2008) 2602–2607.
[29] V. Raghavendra Reddy, Deepti Kothari, Ajay Gupta, S.M. Gupta, Appl. Phys. Lett. 94 (2009) 082505.
[30] B. Kundys, A. Maignan, C. Martin, N. Nguyen, C. Simon, Appl. Phys. Lett. 92 (2008) 112905.